



Phylogeny Reveals Novel HipA-Homologous Kinase Families and Toxin-Antitoxin Gene Organizations

Kenn Gerdes,^a Rene Bærentsen,^b Ditlev E. Brodersen^b

^aCentre of Excellence for Bacterial Stress Response and Persistence, Section for Functional Genomics, Department of Biology, University of Copenhagen, Copenhagen N, Denmark

^bDepartment of Molecular Biology and Genetics, Aarhus University, Aarhus C, Denmark

ABSTRACT Toxin-antitoxin modules function in the genetic stability of mobile genetic elements, bacteriophage defense, and antibiotic tolerance. A gain-of-function mutation of the *Escherichia coli* K-12 *hipBA* module can induce antibiotic tolerance in a subpopulation of bacterial cells, a phenomenon known as persistence. HipA is a Ser/Thr kinase that phosphorylates and inactivates glutamyl tRNA synthetase, inhibiting cellular translation and inducing the stringent response. Additional characterized HipA homologues include HipT from pathogenic *E. coli* O127 and YjjJ of *E. coli* K-12, which are encoded by tricistronic *hipBST* and monocistronic operons, respectively. The apparent diversity of HipA homologues in bacterial genomes inspired us to investigate overall phylogeny. Here, we present a comprehensive phylogenetic analysis of the Hip kinases in bacteria and archaea that expands on this diversity by revealing seven novel kinase families. Kinases of one family, encoded by monocistronic operons, consist of an N-terminal core kinase domain, a HipS-like domain, and a HIRAN (HIP116 Rad5p N-terminal) domain. HIRAN domains bind single- or double-stranded DNA ends. Moreover, five types of bicistronic kinase operons encode putative antitoxins with HipS-HIRAN, HipS, $\gamma\delta$ -resolvase, or Stl repressor-like domains. Finally, our analysis indicates that reversion of *hipBA* gene order happened independently several times during evolution.

IMPORTANCE Bacterial multidrug tolerance and persistence are problems of increasing scientific and medical significance. The first gene discovered to confer persistence was *hipA*, encoding the kinase toxin of the *hipBA* toxin-antitoxin (TA) module of *E. coli*. HipA-homologous kinases phosphorylate and thereby inactivate specific tRNA synthetases, thus inhibiting protein translation and cell proliferation. Here, we present a comprehensive phylogenetic analysis of bacterial Hip kinases and discover seven new families with novel operon structures and domains. Overall, Hip kinases are encoded by TA modules with at least 10 different genetic organizations, 7 of which have not been described before. These results open up exciting avenues for the experimental analysis of the superfamily of Hip kinases.

KEYWORDS high persister A, HipB, HipS, HipT, HIRAN, Stl, GltX, TrpS, kinase

Prokaryotic toxin-antitoxin (TA) modules were discovered due to their ability to stabilize plasmids by killing of plasmid-free cells by a mechanism known as postsegregational killing (1, 2). The mechanism relies on stable protein toxins that are inhibited either by unstable antitoxin RNAs (type I and III TAs) or unstable antitoxin proteins (type II TAs) as long as the plasmid remains in the cell. If, on the other hand, the plasmid is lost, degradation of antitoxin leads to toxin activation and hence, death of the plasmid-free cell. Since their discovery on plasmids, TAs have been identified on a wide range of bacterial and archaeal chromosomes as well (3–5), often in multiple or even large numbers (5–9). For example, *Mycobacterium tuberculosis* carries genes that

Citation Gerdes K, Bærentsen R, Brodersen DE. 2021. Phylogeny reveals novel HipA-homologous kinase families and toxin-antitoxin gene organizations. *mBio* 12:e01058-21. <https://doi.org/10.1128/mBio.01058-21>.

Editor Michael T. Laub, Massachusetts Institute of Technology

Copyright © 2021 Gerdes et al. This is an open-access article distributed under the terms of the [Creative Commons Attribution 4.0 International license](https://creativecommons.org/licenses/by/4.0/).

Address correspondence to Kenn Gerdes, kenn.gerdes5@gmail.com, or Ditlev E. Brodersen, deb@mbg.au.dk.

This article is a direct contribution from Kenn Gerdes, a Fellow of the American Academy of Microbiology, who arranged for and secured reviews by Pierre Genevoux, CNRS-University Paul-Sabatier, and Laurent Falquet, University of Fribourg and Swiss Institute of Bioinformatics.

Received 14 April 2021

Accepted 20 April 2021

Published 1 June 2021

encode ~70 type II TA modules (7, 10, 11), while the plant symbiont *Sinorhizobium meliloti* contains more than 100 (12). The biological functions of chromosome-encoded TAs are debated, but experimental evidence supports at least three roles that are not mutually exclusive: (i) genetic stabilization of chromosome segments or entire chromosomes (13–16), (ii) antiphage defense by abortive infection (17, 18), and (iii) antibiotic tolerance (19–22). Intriguingly, it was recently discovered that bacterial retrons encode a type of three-component TAs that can function as antiphage defense systems, thus supporting the notion that a major function of TAs may in fact be to curb or control bacteriophage infection (23–26). This idea is consistent with the recent observation that environmental or nutritional stress in general does not activate type II TA-encoded toxins (27).

There is evidence supporting that some TAs induce antibiotic tolerance or persistence in bacteria. Persistence is a phenomenon found in all bacteria tested (19, 28–30) and is operationally defined as the subpopulation of a bacterial cells that survive for an extended period of time in the presence of inhibitory concentrations of antibiotics (31). Common to persistence mechanisms is that the phenotype is a stochastic phenomenon and expressed by only a fraction of the cell population at any given time (31, 32). Importantly, persistence is believed to contribute to the recalcitrance of bacterial infections and may thus pose a significant medical problem (30, 33–35). At the mechanistic level, persisters are slow-growing cells that display increased survival rates in the presence of antibiotics (32, 36, 37). In addition, this also buys the bacterial population time to develop true antibiotic resistance (38). Apart from a reduced growth rate, persister cells can also arise from expression of high levels of factors that counter the effects of antibiotics in a small subpopulation of cells (39, 40).

hipA (high persister gene A) of *Escherichia coli* K-12 was the first gene found to be associated with increased persistence based on the identification of the gain-of-function allele *hipA7* in a strain exhibiting increased tolerance toward penicillin (41). The mutant allele, later also found in clinical isolates of uropathogenic *E. coli* (28), exhibits a 100- to 1,000-fold increased level of persistence (32, 42), but even the wild-type *hipBA* module can be shown to confer a modest, but measurable, increase of persistence (28). The *hipA* toxin gene and its upstream *hipB* antitoxin gene constitute a canonical type II TA module encoding two proteins that combine to form an inactive HipBA complex, which, upon degradation of HipB, generates active HipA toxin (Fig. 1A) (43). Consequently, ectopic production of HipA in *E. coli* causes severe growth inhibition that can be reversed by later expression of HipB antitoxin (43). HipBA from both *E. coli* K-12 and *Shewanella oneidensis* MR-1 assemble into heterotetrameric HipA₂B₂ complexes (28, 44–48).

HipA is a so-called Hanks serine-threonine kinase (49, 50) that phosphorylates a conserved serine residue (Ser²³⁹) in glutamyl-tRNA synthetase (GltX) inside its bacterial host, inhibiting the enzyme and thereby aminoacylation of tRNA^{Glu} (51, 52). As a consequence, the ratio of charged to uncharged tRNA^{Glu} decreases, thus stimulating RelA-tRNA^{Glu} complexes to bind the ribosomal A site. Activation of RelA (53) on the ribosome leads to an increase in the cellular (p)ppGpp level triggering the stringent response (42, 51, 54). HipA shares its fold with human cyclin-dependent kinases and maintains all of the conserved motifs necessary for kinase activity (45). The antitoxin HipB contains a classical (Cro-like) helix-turn-helix (HTH) DNA-binding domain (45) and forms a homodimer when in complex with HipA that allows binding to palindromic operator sequences in the *hipBA* promoter region (Fig. 1A). The mechanism of toxin inhibition by HipB has not been fully elucidated, but it appears to differ from most type II systems in that the antitoxin does not interact directly with the toxin active site. Instead, the very C terminus of HipB appears to bind in a pocket on HipA, possibly regulating toxin activity (44). Finally, HipA can inactivate its own kinase activity by autophosphorylation (55), a phenomenon that has been proposed to function in resuscitation of persister cells (46, 56).

HipA homologues are present in many bacteria. For example, the chromosome of the Alphaproteobacterium *Caulobacter crescentus* contains three *hipBA* loci for which

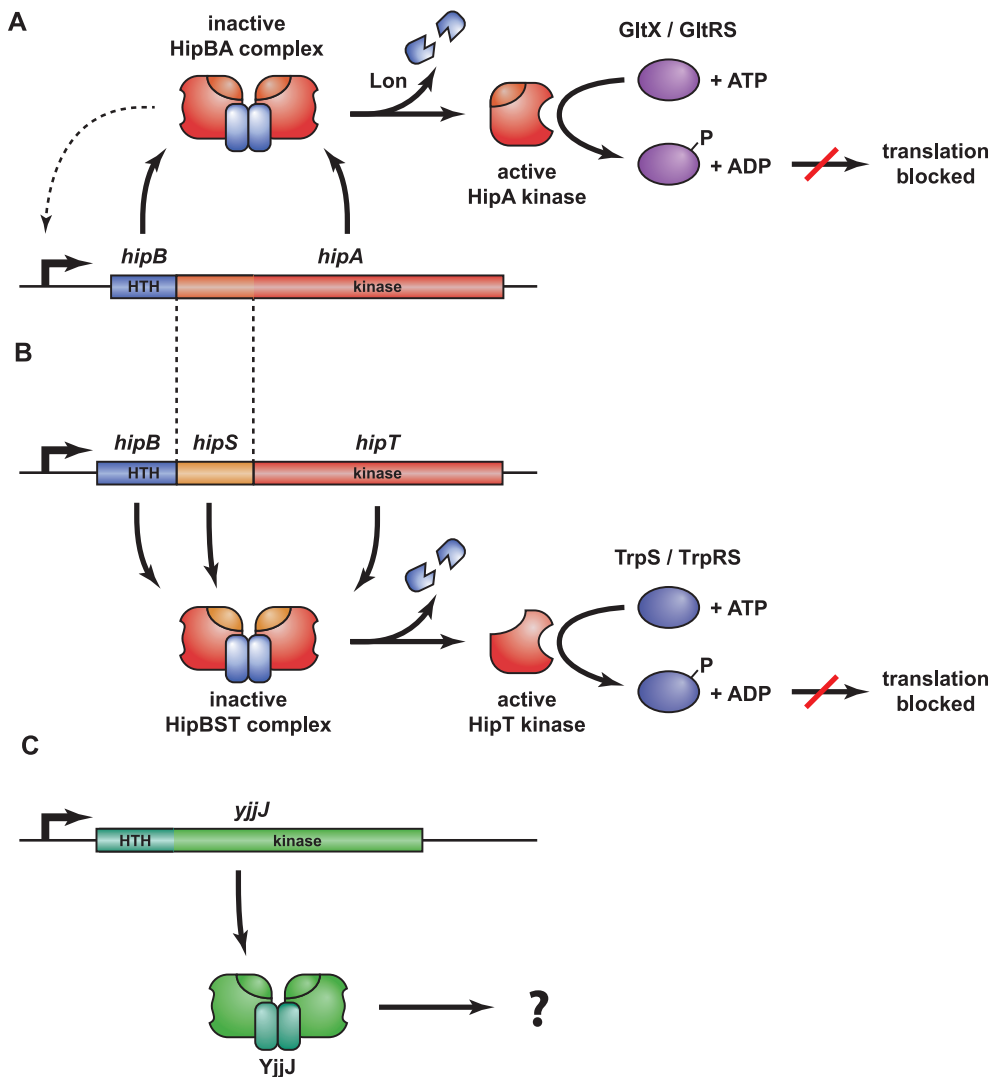


FIG 1 Overview of the *hipBA*, *hipBST*, and *yjjJ* operons and their protein products. (A) *hipBA* encodes the antitoxin HipB (blue) and toxin kinase HipA (red/orange) that form an inactive HipB₂HipA₂ complex that can bind to operators in the promoter region via HTH DNA-binding domains in HipB and thereby autoregulate transcription (dashed line) (28). Upon HipB degradation by Lon protease (88) and activation of HipA, HipA phosphorylates and inhibits glutamine tRNA synthetase (GltX/GltRS), thereby halting translation and inducing the stringent response (51, 52, 54). (B) *hipBST* encodes three proteins, HipB (blue), HipS (orange), and HipT (red) that form an inactive HipBST complex (59). HipS is homologous to the N-subdomain-1 of HipA and functions as the antitoxin that neutralizes HipT (59). Like HipB of HipBA, HipB of HipBST has an HTH domain and augments the inhibition of HipT by HipS but does not function as an antitoxin on its own. Free HipT phosphorylates and inhibits tryptophan tRNA synthetase (TrpS) and thereby halts translation in a similar fashion as HipA. (C) *yjjJ* is a single cistron operon that encodes a HipA-homologous kinase YjjJ (green) that, when overproduced, inhibits cell growth (60). YjjJ, that we coin HipH, has an HTH-domain in its N terminus that may function to bind DNA.

the encoded HipA toxins inhibit protein synthesis upon ectopic expression in all three cases (57). Like their *E. coli* counterpart, HipA₁ and HipA₂ contribute to persistence during stationary phase by phosphorylating aminoacyl-tRNA synthetases *in vivo*: HipA₂ targets lysyl-tRNA synthetase (LysS), tryptophan-tRNA synthetase (TrpS), and GltX, while HipA₁ phosphorylates TrpS and GltX (57). In both cases, the stringent response regulator SpoT (Rel) is required for *hipBA*₁- and *hipBA*₂-mediated persistence. A recent report confirmed that HipA₂ only phosphorylates and inhibits TrpS, whereas LysS and GltX were not found to be phosphorylated (58). Nevertheless, both studies agreed that HipA₂ induces the stringent response and persistence in parallel (57, 58).

We recently described a new family of minimal bacterial kinases, HipT, members of which exhibit sequence similarity with the C-terminal part of HipA but are encoded by

three-gene operons (Fig. 1B) (59). HipT of *E. coli* O127 is functionally similar to HipA and phosphorylates tryptophanyl-tRNA synthetase (TrpS/TrpRS) at two conserved serine residues, inactivating the enzyme. Likewise, ectopic production of *hipT* inhibits cell growth and translation and, consistently, stimulates production of (p)ppGpp (59). The gene immediately upstream of *hipT* encodes a small protein, HipS, that exhibits sequence similarity to the N-terminal part of the larger HipA kinase (Fig. 1B). Surprisingly, HipS neutralizes HipT *in vivo*, and therefore appears to function as the antitoxin of the *hipBST* module. The third component, HipB, encoded by the first gene of the *hipBST* operon (Fig. 1B), contains an HTH domain and is homologous to HipB of HipBA but does not counteract HipT kinase activity directly. Rather, this protein functionally appears to augment the ability of HipS to neutralize HipT (59). The structural and mechanistic details that set the bicistronic and tricistronic Hip kinase systems apart have not yet been elucidated. Finally, *E. coli* K-12 carries genes that encode the HipA homologue YjjJ in a monocistronic operon, thus lacking an adjacent antitoxin gene, which also inhibits cell growth upon induction (Fig. 1C) (60). Interestingly, YjjJ contains a HTH domain at its N terminus that may compensate for the lack of a DNA-binding antitoxin; however, how YjjJ kinase activity is controlled remains unknown.

The discovery of the *hipBST* tricistronic operons (59) as well as the observed diversity among Hip toxin homologues in various bacterial species inspired us to investigate the overall phylogeny of HipA-homologous proteins and their gene families in prokaryotic microorganisms. This led to the discovery of seven novel Hip kinase families, potential antitoxins with novel features such as HIRAN (HIP116 and RAD5 N-terminal) domains with predicted specificity for single-stranded or double-stranded DNA ends and a novel putative two-domain antitoxin family consisting of a HipS-like domain coupled to a HIRAN domain. We also find evidence that HipA-homologous kinases are present in *Archaea*. Together, these results delineate the structural and functional diversity of the family of HipA kinases and suggest directions for future experimental research.

RESULTS AND DISCUSSION

HipA-homologous kinases form a strongly supported, bifurcated phylogenetic tree. The phylogenetic analysis was initiated using HipA and YjjJ of *E. coli* K-12 and HipT of *E. coli* O127 as seed sequences using BLASTP and HMMSEARCH (see Materials and Methods for details). While this revealed a vast number of HipA-homologous kinases within the bacterial domain and a few in the archaeal domain, searches in the *Eukarya* domains did not disclose significant homologues ($E > 10^{-5}$). To analyze the vast number of high-score homologues ($E > 10^{-10}$) systematically, we repeated the search using individual bacterial and archaeal phyla as search spaces (see Fig. S1 in the supplemental material) and retrieved ~1,800 high-scoring Hip homologues. Tenacious curation, including manual inspection of putative neighboring antitoxin genes of each individual kinase gene, removal of incomplete genes, and exclusion of closely related kinases (<5% sequence difference) reduced the number of included kinases to a final set of 1,239 sequences. The majority of these are from the phylum *Proteobacteria* (70%) while they are also frequently observed among *Actinobacteria* (13%), *Firmicutes* (5%), and *Spirochaetes* (2%) (see Table S1 in the supplemental material). Using these sequences, we generated a phylogenetic tree, called the “Hip Tree” (Fig. 2A). Fully annotated and bootstrapped versions of the Hip Tree are shown in Fig. S2A and S2B, while a full breakdown of the phylogeny of the kinases is given in Table S2A. The Hip Tree consists of 11 main clades (clades I to XI) all supported by high statistical confidence levels (Table 1). The tree is bifurcated with one branch containing main clades I through X, while the other branch consists of the diverse main clade XI (Fig. 2A). In Fig. 2A, the colors of the clades (shown as triangles) reflect kinases encoded by TA modules with identical genetic organization, as explained in the next section. In other words, each differently colored triangle in Fig. 2A reflects HipA-homologous kinases encoded by TA modules with a different genetic organization.

HipA-homologous kinases are encoded by 10 different genetic organizations. By careful investigation of the sequence data set in Table S1, we found that a

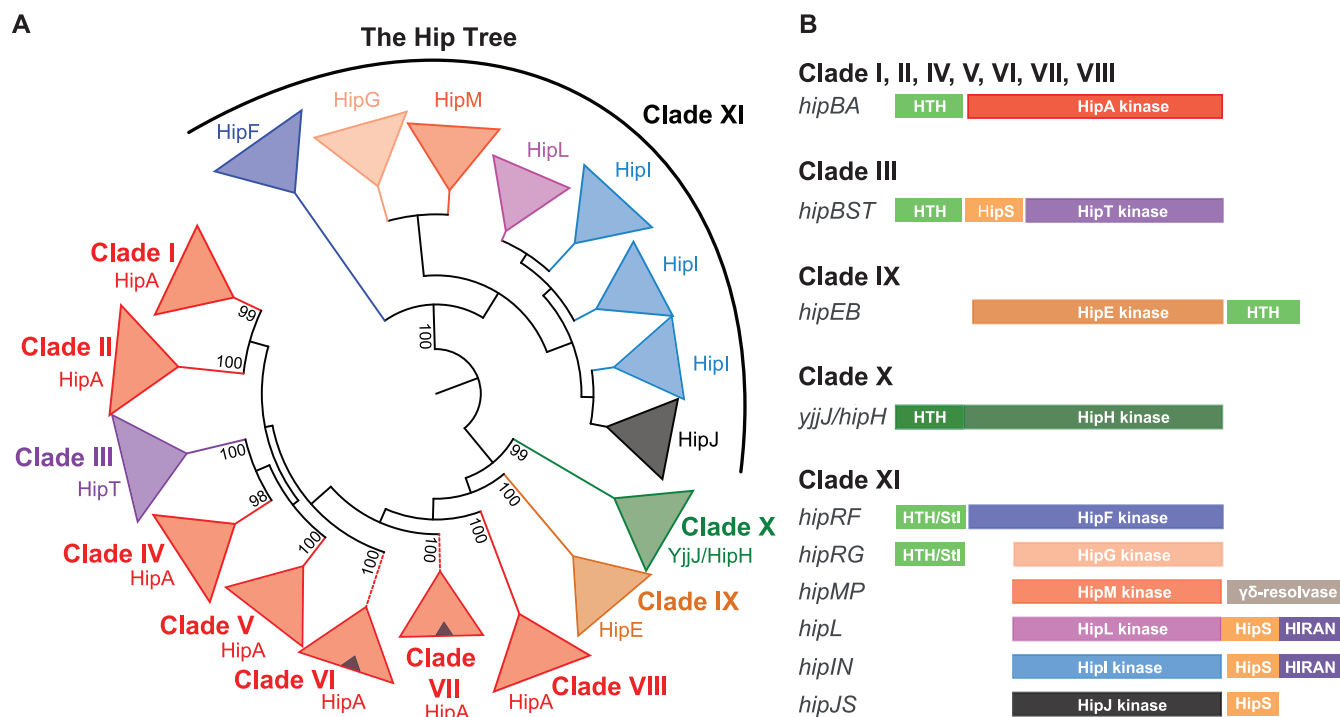


FIG 2 Phylogeny and genetic contexts of HipA-homologous kinases. (A) Simplified phylogenetic tree covering 1,239 HipA-homologous kinases (the “Hip Tree”) (see Fig. S2 in the supplemental material for details). The Hip Tree was divided into 11 main clades I to XI. The coloring of the Hip Tree reflects the genetic contexts that encode the kinases such that each color corresponds to a distinct kinase family encoded by a distinct type of TA module. All main clades are monophyletic except clade XI that consists of six different kinase families. Small blue triangles within the red triangles of main clades VI and VII symbolize subclades of kinases encoded by TA modules with a reversed gene order relative to *hipBA*—that is—with the gene order *hipAB*. The Hip Tree was visualized by iTOL (82). (B) Genetic organizations of the TA modules encoding the 1,239 HipA-homologous kinases. The various types of genetic organization were obtained by manual inspection of the genes upstream and downstream of the kinase genes listed in Table S1 in the supplemental material. The coloring of the Hip kinases in panel B follows the coloring of the clades in panel A. Putative antitoxins with helix-turn-helix (HTH) domains are colored light green. Stl/HTH, putative antitoxins containing HTH domain and a domain with structural similarity to the “polyamorous” repressor Stl encoded by *Staphylococcus aureus*; HipS, HipS-like; HIRAN, HIP116 Rad5p N-terminal domain.

consistent and biological meaningful definition of “Hip kinase family” can be based on the genetic context encoding the kinases. Using this classification, we identified a total of 10 Hip kinase families encoded by TA modules with 10 different genetic organizations (Fig. 2B). The frequencies of the TA modules with different genetic organizations are given in Table S2B.

Using this classification, all HipA kinases encoded by *hipBA* modules with an upstream HipB HTH antitoxin gene cluster together in clades I, II, and IV to VIII. Experimentally characterized *hipBA* modules from *E. coli* K-12 and *C. crescentus* are all in clade I (Fig. S2A). Interestingly, clades VI and VII each contain a subclade that have a reversed gene order (i.e., *hipAB*), indicating that gene reversion occurred independently several times during evolution (shown as blue triangles within red triangles in Fig. 2A and as branches with dashed lines in Fig. S2A). Similarly, clade IX consists entirely of kinases encoded by operons with a reversed gene order relative to *hipBA*, and the deep branching of this clade warrants the definition of a new kinase family that we call HipE (Fig. 2A). HipE kinases are encoded by *hipEB* operons that also encode putative HipB antitoxins with HTH domains (Fig. 2B). Clade III consists solely of HipT kinases encoded by *hipBST* operons, including the characterized locus from *E. coli* O127, while clade X consists entirely of YjjJ-like kinases encoded by monocistronic operons. Interestingly, clade XI is highly diverse and contains no less than six kinase families (Fig. 2A) encoded by different genetic contexts (Fig. 2B). To standardize the nomenclature, all genes encoding putative antitoxins with HTH domains have been named HipB except for HipB of *hipBST* and HipR of *hipRF* and *hipRG*. In all cases investigated, HipB functions as both an antitoxin and an autoregulator of transcription with the exception of the HipB protein encoded by the *hipBST* operons, which autoregulates transcription

TABLE 1 Overview of the clades of the Hip Tree consisting of 1,239 kinases^a

Clade	No. of kinase genes	TA gene organization ^b	Experimentally analyzed TA modules	Cellular target(s) of toxin	GenBank ID ^c	Reference(s)
I	712	<i>hipBA</i>	<i>hipBA</i> of <i>E. coli</i> K-12 <i>hipBA</i> ₁ of <i>C. crescentus</i> <i>hipBA</i> ₂ of <i>C. crescentus</i> <i>hipBA</i> ₃ of <i>C. crescentus</i> <i>hipBA</i> of <i>S. oneidensis</i> MR-1	GltX Unknown or GltX and LysS LysS or GltX, LysS and TrpS ^e Unknown ^e Unknown	NP_416024.1 (440) ACL93947.1 (423) ACL96286.1 (444) WP_010920611.1 (435) ^d AAN53784.1 (433)	47, 51, 52, 57, 58
II	73	<i>hipBA</i>	None			
III	48	<i>hipBA</i>	<i>hipBST</i> of <i>E. coli</i> O127 <i>H. influenzae</i> KW20 <i>T. auensis</i> DSM9187	TrpS TrpS TrpS	WP_015879003.1 (342) NP_438824.1 (343) CAS11333.1 (335)	59
IV	14	<i>hipBA</i>	None			
V	9	<i>hipBA</i>	None			
VI	36	<i>hipBA</i>	None			
VII	132	<i>hipAB</i> and <i>hipAB</i>	None			
VIII	21	<i>hipBA</i>	None			
IX	12	<i>hipEB</i>	None			
X	101	<i>hipH/yjjJ</i>	<i>hipH/yjjJ</i>		P39410.1 (443)	60
XI	81	<i>hipRF</i> , <i>hipRG</i> , <i>hipMP</i> , <i>hipL</i> , <i>hipIN</i> , and <i>hipJS</i>	None			

^aData compiled from Table S1 in the supplemental material.

^bGene organization refers to information retrieved from Table S1 and visualized schematically in Fig. 2B.

^cGenBank identifiers (IDs) or accession numbers of the kinases are from Table S1 and their position in amino acids in the Hip Tree visualized in Fig. S2A and S2B in the supplemental material.

^d*hipBA*₃ of *C. crescentus* previously had the accession number NP_421566.1 and was used in Table S1.

^eThe substrate of HipA₁ is either unknown (58) or GltX plus LysS (57), while the substrate of HipA₂ is either TrpS (58) or GltX, LysS plus TrpS (57).

but does not function as an antitoxin as mentioned above (20, 59). As described later, HipR-encoded *hipRF* and *hipRG* operons also contain a HTH domain but exhibits structural similarity with the StI repressor.

Conserved HipA kinases appear to contain functionally significant differences.

Clade I contains the “classical” bacterial HipA kinases with known cellular targets, HipA of *E. coli* K-12, HipA₁ and HipA₂ of *C. crescentus*, together with their close homologues. An alignment of representative sequences of subclades containing HipA, HipA₁, and HipA₂ kinases reveals, as expected, the four canonical core kinase motifs: the Gly-rich loop, the activation loop, the catalytic motif, and the Mg²⁺-binding motif (Fig. S3). The alignment also reveals a number of insertions (ω 1 to ω 6) and deletions (Δ 1 to Δ 3), also called “indels” in the two *C. crescentus* HipA (HipA_{Cr}) subclades relative to the *E. coli* K-12 HipA (HipA_{E. coli K-12}) subclade (Fig. S3). Figure 3A shows a schematic overview of HipA indicating the positions of the indels relative to the core kinase motifs in the primary sequences, while Fig. 3B and C show a mapping of the HipA₁- and HipA₂-specific indels as well as regions of high sequence divergence onto the structure of HipA of *E. coli* K-12. Interestingly, despite being distant in the primary sequence, the two largest deletions in *E. coli* HipA (Δ 2 and Δ 3) are adjacent in the tertiary structure (Fig. 3B and C) and close to the γ -phosphate of ATP. Additionally, both *C. crescentus* HipA kinases share a C-terminal region of high sequence divergence that maps to solvent-exposed residues of a surface helix (Fig. 3A), while HipA₂ has an additional unique region of divergence (Fig. 3C). Studies of eukaryotic cyclin-dependent kinases have shown that the homologous region where Δ 2, Δ 3, and both regions of divergence are situated is involved in target binding (61), raising the possibility that the differences observed relate to differences in target specificity. Finally, we note that HipA₂ has several regions (ω 1', ω 2', and ω 3') not present in HipA (Fig. 3A and Fig. S3) concentrated in the region that interacts with the very C terminus of HipB in the *E. coli* HipBA structure (Fig. 3C), thus potentially affecting the mechanism by which the antitoxin interacts with and inhibits the cognate kinase.

All HipT kinases lack the canonical N-terminal subdomain. Main clade III consists exclusively of HipT kinases (Fig. 2). As shown before, the sequences of the HipT kinases of *E. coli* O127, *Haemophilus influenzae*, and *Tolomonas auensis* align colinearly with the

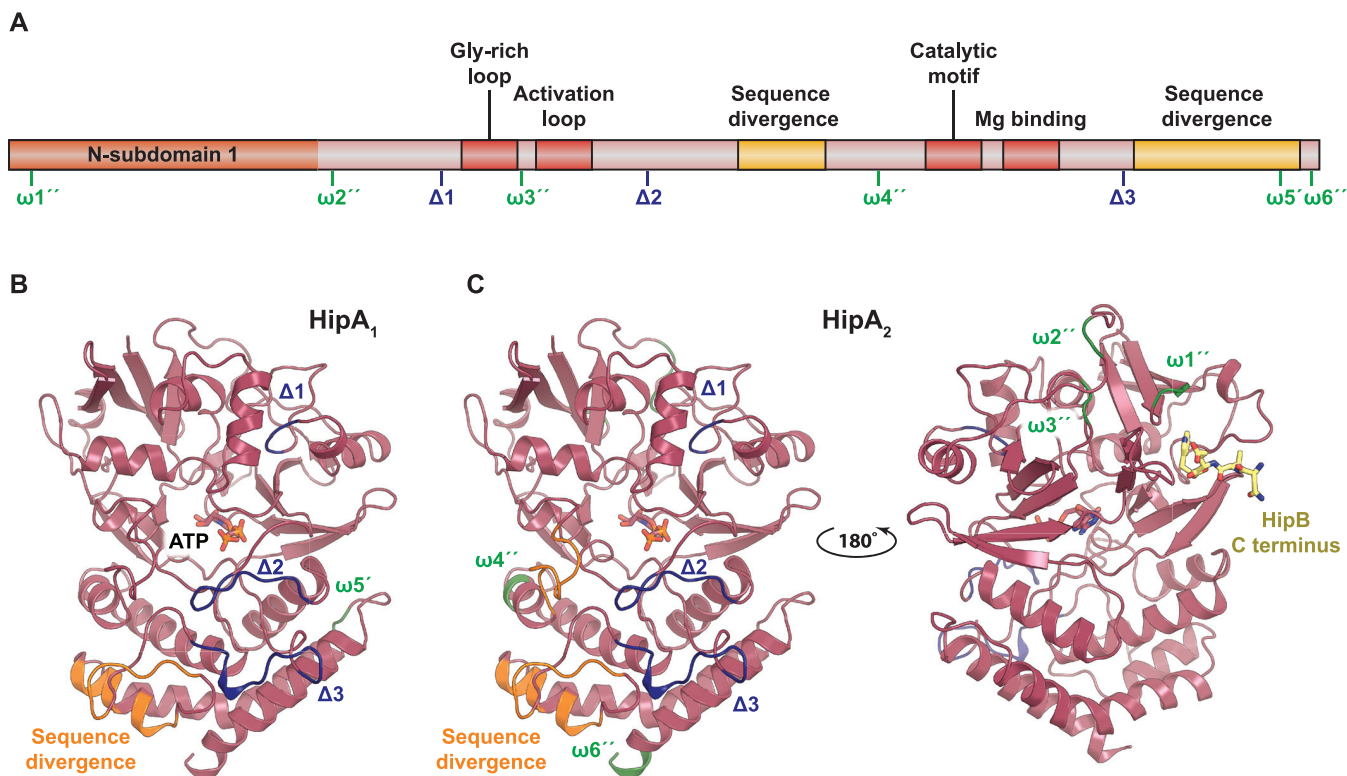


FIG 3 Structural mapping of insertions and deletions observed in characterized HipA kinases. (A) Schematic overview of HipA showing the conserved regions (the Gly-rich loop, activation loop, catalytic motif, and Mg-binding motif) in red as well as insertions (ω [green]) and deletions (Δ [blue]) in *C. crescentus* HipA₁ and HipA₂ relative to HipA from *E. coli* K-12 based the sequence alignment shown in Fig. S3. An insertion in HipA₁ relative to HipA is denoted $\omega 5'$, while insertions in HipA₂ relative to HipA are marked $\omega 1''$, $\omega 2''$, $\omega 3''$, $\omega 4''$, and $\omega 6''$. Deletions in HipA₁ and HipA₂ relative to HipA are marked $\Delta 1$, $\Delta 2$, and $\Delta 3$. Regions of high sequence divergence are shown in yellow. (B) Mapping of the insertions and deletions in HipA₁ onto the structure of HipA of *E. coli* K-12 (PDB accession no. 3FBR) using the same nomenclature and color scheme as in panel A (45). ATP is shown with colored sticks. (C) Mapping of the insertions and deletions in HipA₂ onto the structure of HipA. Note that the insertions $\omega 1''$ and $\omega 3''$ in HipA₂ are located close to the region that in HipA interacts with the C terminus of HipB (yellow sticks) and could perhaps affect antitoxin activity.

C-terminal part of *E. coli* K-12 HipA (Fig. S4A) but lack the canonical ~ 100 -amino-acid (aa) N-subdomain-1 that serves as a lid on top of the core kinase domain in HipA (59). Nevertheless, the four conserved Hip kinase motifs (Gly-rich loop, activation loop, catalytic motif, and Mg²⁺-binding motif) are conserved in the HipTs, as well as a serine adjacent to the Gly-rich loop that is subject to autophosphorylation in both HipT and HipA (46, 59). We showed previously that HipS, which is encoded immediately upstream of HipT, functions as the antitoxin of *hipBST* modules and that this protein exhibits sequence similarity to the N-terminal domain of HipA (59) (Fig. S4A and S4B). In other words, the “missing” N-subdomain-1 of HipT appears to be encoded immediately upstream and thus in a similar genomic location relative to the core kinase domain as in HipA, which suggests that the gene has been split (or merged) at some point during evolution. However, the functional and structural implications of this difference with respect to kinase activation and regulation are not yet understood.

YjjJ kinases contain an N-terminal HTH domain. YjjJ of *E. coli* K-12 is a HipA homologue encoded by a monocistronic operon and thus “lacking” a closely linked antitoxin or DNA-binding HipB-like gene. Instead, YjjJ has a ~ 100 -aa N-terminal extension containing a helix-turn-helix (HTH) domain (residues 15 to 34) that potentially could function as a *cis*-acting antitoxin, a property previously found with other type II modules (62). To maintain a uniform nomenclature, we propose here to rename YjjJ kinases HipH (H for HTH domain) as these constitute the monophyletic clade X in the Hip Tree (Fig. 2A). To avoid alignment of nonhomologous domains, we chose to align subclade HipH_{*E. coli* K-12} with HipT_{*E. coli* O127} because HipT lacks the ~ 100 -aa N-terminal domain present in HipA but has all the canonical kinase domains. As seen from Fig. 4,

HipH and HipT kinases align colinearly with respect to the four conserved kinase motifs, while the N terminus of HipH forms a separate HTH domain. Moreover, HipH kinases contain two conserved serine residues near the Gly-rich loop, raising the possibility that they are regulated through autophosphorylation in a way similar to HipT (59).

Main clade XI consists of kinases belonging to six different families. The kinases in main clade XI of the Hip Tree are encoded by six different genetic contexts and define six novel Hip kinase families (Fig. 2A and B). All six subclades are separated by high bootstrap values, supporting that their separation into novel kinase families is phylogenetically justified (Fig. S5). The six families encompass four families of short kinases (HipG, HipM, HipI, and HipJ), one longer variant (HipF) similar in size to HipA and a “long” kinase family (HipL) (Fig. 2B). In the following, we describe these six new types of kinase-encoding TA modules.

The HipG, HipM, HipI, and HipJ families contain the core kinase domain. The HipG, HipI, HipJ, and HipM kinases are all phylogenetically closely related and are, on average, even smaller than the HipT kinases (279 to 321 aa versus 291 to 346 aa, respectively) (Table S1 and Fig. S5). A sequence alignment of representatives of these families confirms that they contain the four conserved core Hip sequence motifs are thus likely active kinases (Fig. S6). However, like HipT, these kinases lack the N-subdomain-1 present in HipA, HipE, and HipF and consequently, the Gly-rich loop is located close to the N termini (Fig. S6). The kinases in the HipG group do not have a conserved serine or threonine adjacent to the Gly-rich loop, suggesting they are probably not regulated by autophosphorylation in a way similar to HipA. In contrast, members of the other families (HipM, HipI, and HipJ) mostly have either Ser or Thr near the Gly-rich loop, suggesting on the other hand that they may be regulated in this way. We note that HipI kinases constitute four separate subclades of the phylogenetic reconstruction of main clade XI (Fig. 2A). Three of the subclades consists of kinases from *Actinobacteria* and *Firmicutes* while the fourth consists of a mix of kinases from *Proteobacteria* and *Cyanobacteria* (Fig. S5).

HipF and HipG kinases have putative antitoxins related to polyamorous repressor Stl. HipF and HipG kinases are encoded in operons with putative antitoxins that we call HipR (Fig. 2B). Interestingly, Phyre2 (63) predicts HipR to be structurally related to the two-domain transcriptional repressor Stl encoded by *Staphylococcus aureus* superantigen-carrying pathogenicity islands (*SaPI*). Stl has an HTH domain and maintains integration of *SaPI* elements in the bacterial chromosome by transcriptionally repressing genes essential for element excision and replication (64). *SaPI* excision and replication are induced by invading phages via specific interaction between Stl and nonessential phage proteins (65–69). These observations allow us to hypothesize that phage proteins could potentially activate HipF and/or HipG kinases during infection via interaction with HipR. Under this model, activation of the kinases induces abortive phage infection by inhibition of translation via phosphorylation of an essential component of the protein synthesis apparatus, thus eliciting phage resistance. This possibility can now be tested experimentally.

Putative HipN antitoxins consist of a HipS-like and a HIRAN domain. The genes encoding HipM, HipI, and HipJ kinases all have downstream genes coding for putative antitoxins (Fig. 2B). The putative antitoxin HipN encoded by *hipN* is a two-domain protein consisting of an N-terminal HipS-like domain (Fig. S7A) and a C-terminal HIRAN domain (Fig. S8A). The HipS-like domain of HipN may function to neutralize its cognate HipI kinase as is the case of HipS encoded by *hipBST* (59). A possible function of the HIRAN domain of HipN is discussed below.

A second family of putative HipS antitoxins. *hipJS* modules encode a HipJ kinase and a putative antitoxin HipS that exhibits similarity to HipS of *hipBST* (Fig. S7A). Thus, similarly to HipT (59), HipJ may be neutralized by its cognate HipS. As noted above, HipS and HipS-like domains exhibit sequence similarity with the ~100-aa N-subdomain-1 of HipA, and this domain was therefore included in the alignment of the HipS antitoxins and HipS-like domains (Fig. S7A). The phylogenetic tree based on the HipS and HipS-like sequences is bifurcated, with HipS encoded by *hipBST* and *hipJS* branch together with N-subdomain-1 of HipA, while the HipS-like sequences encoded by *hipL* and *hipN* generate a

distinct second branch (Fig. S7B). HipJ kinases are closely related to HipI kinases (Fig. S5), and it is tempting to speculate that *hipJS* modules evolved from *hipIN* modules by deletion of the HIRAN domain of HipN antitoxins (Fig. 2B).

HipL kinases contain both HipS-like and HIRAN domains. HipL kinases, encoded by monocistronic operons, form a single subclade of main clade XI that is further divided into two subclades (Fig. S5). The two subclades consist of HipL kinases from Gram-positive and Gram-negative bacteria. Their sequences are clearly distinct, with many subclade-specific insertions and deletions in the kinase core domain (Fig. S8B). Alignment of HipL and HipA reveals that HipL maintains the four, conserved core kinase motifs and has a large C-terminal extension of ~200 aa of which the ~100 aa at the extreme C terminus are annotated at GenBank as a HIRAN domain (Fig. S8C). Like the small kinases, HipL kinases lack the N-subdomain-1 of ~100 aa relative to the core kinase domain of HipA (Fig. S8C). Unexpectedly, however, the ~100-aa domain located between the core kinase domain and the C-terminal HIRAN domain exhibits sequence similarity with HipS (Fig. S8D). The N-terminal sequences of HipA also align well with the HipS-like domain of HipL (Fig. S8E), consistent with the fact that HipS exhibits sequence similarity with the N-subdomain-1 of HipA (Fig. S4B). In summary, HipL kinases are three-domain proteins consisting of an N-terminal kinase core domain, a HipS-like domain, and a C-terminal HIRAN domain (Fig. 2B and Fig. S8C). We note the possibility that the HipS-like domain may be involved in regulating the kinase activity of HipL, reminiscent of how HipS regulates the kinase activity of HipT (59).

The HIRAN domains of HipL and HipN may bind DNA. The presence of HIRAN domains in both HipL kinase and the putative antitoxins HipN is interesting, not least because HIRAN domains can bind DNA. Moreover, the HIRAN domains of HipL kinases and HipN antitoxins are in both cases joined with a HipS-like domain (Fig. 2B). HIRAN domains have previously been identified in eukaryotic multidomain DNA repair proteins (70). Experimentally analyzed HIRAN domains bind single-stranded or double-stranded DNA ends (71, 72). Structural studies of human helicase-like transcription factor (HLTF), a DNA helicase implicated in remodeling of replication forks, including fork regression and restart (73), revealed the residues required for DNA binding (72) (Fig. 5A and B). Due to a high sequence divergence, we decided to split the HIRAN domains of the HipN homologues based on their phylogenetic origin (Fig. 5C and Fig. S8A). Most of the HIRAN domains retained the majority of the sequence motifs that interact with DNA, with the exception of HipN from *Actinobacteria*. A study of the HIRAN domain of human HLTF showed that Phe142 (NAE) is required for binding to duplex DNA because it stacks with nucleobases of the other strand (72) (Fig. 5B). Importantly, most of the bacterial HIRAN domains lack a conserved Phe at this position (Fig. 5C), raising the possibility that the HIRAN domains in HipN and HipL interact with single-stranded DNA (ssDNA).

The function(s) of the HIRAN domains of HipL and HipN is, of course, unknown. One attractive possibility is that the HIRAN domains of HipL and HipN recognize DNA ends (ssDNA or double-stranded DNA [dsDNA] or both) of invading phages or phage DNA replicative intermediates that, in turn, leads to activation of the HipL and HipI kinases. Activation of the kinases could lead to phosphorylation and inhibition of an essential cellular component, thereby triggering abortive phage infection. Abortive phage infection is a common biological function of TA modules (74, 75), and the possibility that *hipL* and *hipIN* function to curb phage infection can now be tested experimentally.

A putative antitoxin with a $\gamma\delta$ -resolvase-like domain. A final variation among the Hip kinases is found for the *hipMP* modules, which encode a HipM kinase that is short and closely related to HipG kinases (Fig. 2A) and a putative HipP antitoxin that exhibits similarity to $\gamma\delta$ -resolvases (Fig. 2B). Bacterial $\gamma\delta$ -resolvases are transposon-encoded enzymes that catalyze recombination within a complex nucleoprotein structure during site-specific DNA recombination and thus have the capability to bind DNA (76). Interestingly, $\gamma\delta$ -resolvases are structurally related to 5'-3' exonucleases active on RNA, which may also provide clues to the role of this domain in the context of Hip kinases (77). By analogy with other *hipBA* modules (28, 78), we therefore postulate that

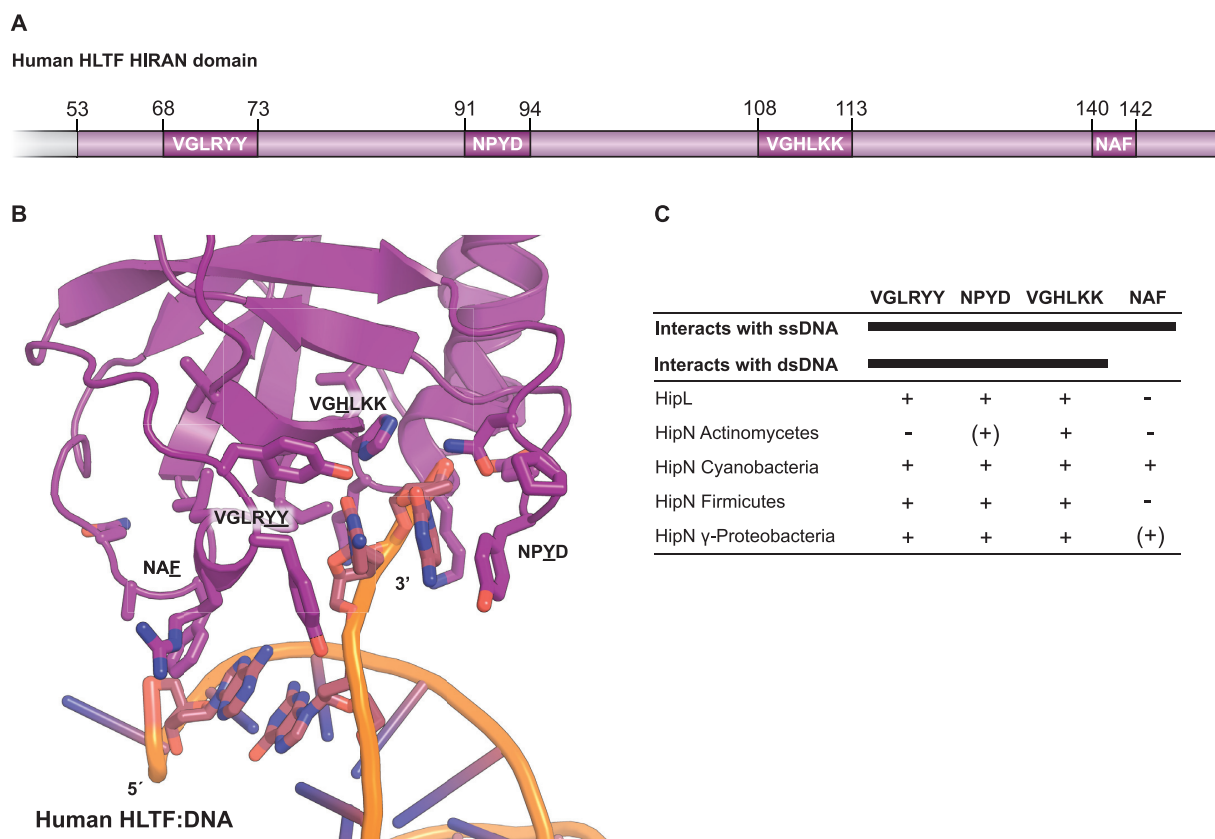


FIG 5 Comparative analysis of HIRAN domains. The HIRAN domains of HipL and HipN have sequence motifs required for DNA binding. (A) Schematic overview of the HIRAN domain found in human helicase-like transcription factor (HLTF) showing the relative positions and sequences involved in ssDNA and dsDNA binding (72). (B) Structure of the human HLTF HIRAN domain with the four regions necessary for DNA binding shown as sticks (PDB accession no. 4XZF) (72). (C) Overview of sequence motifs present (+) or absent (-) in homologues of HipL and HipN.

HipP functions as antitoxin in the *hipMP* systems and may bind DNA to autoregulate transcription as seen for many type II TA systems.

Conclusion. In addition to the three known kinase families HipA, HipT, and YjjJ/HipH, we discover here seven novel Hip kinase families encoded by different genetic contexts. Kinases of one family, HipE, are encoded by TA operons with a reversed gene order relative to *hipBA*, while kinases of families HipF and HipG have putative StI-homologous antitoxins that may be regulated by proteins encoded by attacking phages. Kinases of one family, HipJ, are associated with HipS domain putative antitoxins that, similar to HipS of *hipBST*, may interact with and neutralize their cognate kinase toxins. Kinases of yet another family, HipI, are associated with putative antitoxins that consist of a HipS-like domain and a HIRAN DNA-binding domain, while HipJ kinases are associated with putative antitoxins exhibiting similarity with $\gamma\delta$ -resolvases. Finally, HipL kinases, encoded by monocistronic operons, consist of an N-terminal core kinase domain, an internal HipS-like domain, and a C-terminal HIRAN DNA-binding domain. The latter two domains of HipL may function in regulating its kinase activity. Our analysis presented here builds a foundation for the future experimental analysis of HipA-homologous kinases.

MATERIALS AND METHODS

Data sampling. As of December 2019, HipA and HipH/YjjJ of *E. coli* K-12 and HipT of *E. coli* O127 were used as seeds in BLASTP searches at <https://blast.ncbi.nlm.nih.gov/>, using the bacterial phyla shown in Fig. S1 as search spaces. HMMSEARCH at www.ebi.ac.uk (79) was used to expand poorly populated clades. In total, $\approx 1,800$ Hip sequences were retrieved ($E > 10^{-10}$) and curated manually such that every Hip kinase sequence retained satisfied the following criteria. (i) The Hip kinase gene should encode a full-length kinase with the four canonical kinase motifs (Gly-rich loop, activation loop, catalytic motif, and Mg^{2+} binding domain), as determined from a multiple-sequence alignment (MSA). (ii) Kept kinases

should be encoded by a gene with an adjacent upstream or downstream putative antitoxin gene. (iii) In general, the adjacent, putative antitoxin gene should encode a DNA-binding protein (although this criterion is not satisfied by HipJ proteins). In Table S1 in the supplemental material, kept kinases are less than 95% identical to any other kept kinase. By this scrutiny, the initial gene set was reduced to 1,239 Hip gene modules (Table S1 and Fig. 2).

Toxin-antitoxin module gene organization. The gene organizations shown in Fig. 1 were deduced by manual inspection of genes neighboring the Hip kinase genes of Table S1.

Sequence alignments and phylogenetic tree reconstruction. Sequence alignments were generated by Clustal Omega (80) at www.ebi.ac.uk and imported into Jalview (81). Protein sequence alignments in Jalview 2.11.0 were exported as vector files (EPS or SVG formats) and imported into Adobe Illustrator CS6, annotated, and saved in PDF format for publication. Phylogenetic trees were visualized using iTOL (82). Reconstruction of phylogenetic trees was accomplished using IQ-TREE that uses the maximum likelihood approach and Ultrafast bootstrapping via the CIPRES module in Genious Prime (83–85). The kinase sequence alignments used in the reconstruction of the three phylogenetic trees that we present had the following characteristics. (i) The sequence alignment of the 1,239 kinases (Fig. S2) has 1,556 columns, 1,511 distinct patterns, 1,172 parsimony-informative sites, 172 singleton sites, and 211 constant sites. (ii) The sequence alignment of the 81 sequences of main clade XI (Fig. S5) has 785 columns, 761 distinct patterns, 650 parsimony-informative sites, 58 singleton sites, and 77 constant sites. (iii) The sequence alignment of the 112 HipS and HipS-like sequences (Fig. S7B) has 170 columns, 170 distinct patterns, 146 parsimony-informative sites, 16 singleton sites, and 8 constant sites. The alignment of the HipS and HipS-like sequences has fewer singleton and constant sites, thus explaining the low bootstrap values (Fig. S7B).

Structure similarity searches were done using Phyre2 (63) (<http://www.sbg.bio.ic.ac.uk/phyre2/>) and mapping of deletions and insertions on existing structures using PyMOL. HTH motifs were identified by two different algorithms, EMBOSS (86) and HELIX-TURN-HELIX MOTIF PREDICTION (87).

SUPPLEMENTAL MATERIAL

Supplemental material is available online only.

FIG S1, PDF file, 2.5 MB.

FIG S2, PDF file, 2.1 MB.

FIG S3, JPG file, 2.5 MB.

FIG S4, PDF file, 2.7 MB.

FIG S5, PDF file, 0.3 MB.

FIG S6, JPG file, 2.8 MB.

FIG S7, JPG file, 2.6 MB.

FIG S8, JPG file, 2.8 MB.

TABLE S1, TXT file, 0.7 MB.

TABLE S2, DOCX file, 0.02 MB.

ACKNOWLEDGMENTS

We thank Boris Macek (Proteome Center Tübingen, University of Tübingen, Germany) and Yong E. Zhang (Department of Biology, University of Copenhagen, Denmark) for critical comments on the manuscript.

This work was supported by a Novo Nordisk Foundation Ascending Investigator grant to D.E.B. (grant NNF18OC0030646), a Center-of-Excellence grant from the Danish Natural Research Foundation to K.G. (DNRF120), and a personal Laureate Research Grant from the Novo Nordisk Foundation to K.G.

REFERENCES

- Hiraga S, Ogura T, Mori H, Tanaka M. 1985. Mechanisms essential for stable inheritance of mini-F plasmid. *Basic Life Sci* 30:469–487.
- Gerdes K, Rasmussen PB, Molin S. 1986. Unique type of plasmid maintenance function: postsegregational killing of plasmid-free cells. *Proc Natl Acad Sci U S A* 83:3116–3120. <https://doi.org/10.1073/pnas.83.10.3116>.
- Gerdes K, Bech FW, Jorgensen ST, Lobner-Olesen A, Rasmussen PB, Atlung T, Boe L, Karlstrom O, Molin S, von Meyenburg K. 1986. Mechanism of post-segregational killing by the hok gene product of the parB system of plasmid R1 and its homology with the relF gene product of the E. coli relB operon. *EMBO J* 5:2023–2029. <https://doi.org/10.1002/j.1460-2075.1986.tb04459.x>.
- Masuda Y, Miyakawa K, Nishimura Y, Ohtsubo E. 1993. chpA and chpB, Escherichia coli chromosomal homologs of the pem locus responsible for stable maintenance of plasmid R100. *J Bacteriol* 175:6850–6856. <https://doi.org/10.1128/jb.175.21.6850-6856.1993>.
- Blower TR, Short FL, Rao F, Mizuguchi K, Pei XY, Fineran PC, Luisi BF, Salmond GP. 2012. Identification and classification of bacterial Type III toxin-antitoxin systems encoded in chromosomal and plasmid genomes. *Nucleic Acids Res* 40:6158–6173. <https://doi.org/10.1093/nar/gks231>.
- Gerdes K, Wagner EG. 2007. RNA antitoxins. *Curr Opin Microbiol* 10:117–124. <https://doi.org/10.1016/j.mib.2007.03.003>.
- Pandey DP, Gerdes K. 2005. Toxin-antitoxin loci are highly abundant in free-living but lost from host-associated prokaryotes. *Nucleic Acids Res* 33:966–976. <https://doi.org/10.1093/nar/gki201>.
- Jørgensen MG, Pandey DP, Jaskolska M, Gerdes K. 2009. HicA of Escherichia coli defines a novel family of translation-independent mRNA interferases in bacteria and archaea. *J Bacteriol* 191:1191–1199. <https://doi.org/10.1128/JB.01013-08>.
- Lepplae R, Geeraerts D, Hallez R, Guglielmini J, Dreze P, Van Melderen L. 2011. Diversity of bacterial type II toxin-antitoxin systems: a

- comprehensive search and functional analysis of novel families. *Nucleic Acids Res* 39:5513–5525. <https://doi.org/10.1093/nar/gkr131>.
10. Ramage HR, Connolly LE, Cox JS. 2009. Comprehensive functional analysis of *Mycobacterium tuberculosis* toxin-antitoxin systems: implications for pathogenesis, stress responses, and evolution. *PLoS Genet* 5:e1000767. <https://doi.org/10.1371/journal.pgen.1000767>.
 11. Sala AJ, Bordes P, Ayala S, Slama N, Tranier S, Coddeville M, Cirinesi A-M, Castanie-Cornet M-P, Mourey L, Genevaux P. 2017. Directed evolution of SecB chaperones toward toxin-antitoxin systems. *Proc Natl Acad Sci U S A* 114:12584–12589. <https://doi.org/10.1073/pnas.1710456114>.
 12. Milunovic B, diCenzo GC, Morton RA, Finan TM. 2014. Cell growth inhibition upon deletion of four toxin-antitoxin loci from the megaplasmids of *Sinorhizobium meliloti*. *J Bacteriol* 196:811–824. <https://doi.org/10.1128/JB.01104-13>.
 13. Szekeres S, Dauti M, Wilde C, Mazel D, Rowe-Magnus DA. 2007. Chromosomal toxin-antitoxin loci can diminish large-scale genome reductions in the absence of selection. *Mol Microbiol* 63:1588–1605. <https://doi.org/10.1111/j.1365-2958.2007.05613.x>.
 14. Wozniak RA, Waldor MK. 2009. A toxin-antitoxin system promotes the maintenance of an integrative conjugative element. *PLoS Genet* 5:e1000439. <https://doi.org/10.1371/journal.pgen.1000439>.
 15. Yuan J, Yamaichi Y, Waldor MK. 2011. The three *Vibrio cholerae* chromosome II-encoded ParE toxins degrade chromosome I following loss of chromosome II. *J Bacteriol* 193:611–619. <https://doi.org/10.1128/JB.01185-10>.
 16. Yao X, Chen T, Shen X, Zhao Y, Wang M, Rao X, Yin S, Wang J, Gong Y, Lu S, Le S, Tan Y, Tang J, Fuqan H, Li M. 2015. The chromosomal SezAT toxin-antitoxin system promotes the maintenance of the SsPI-1 pathogenicity island in epidemic *Streptococcus suis*. *Mol Microbiol* 98:243–257. <https://doi.org/10.1111/mmi.13116>.
 17. Fineran PC, Blower TR, Foulds IJ, Humphreys DP, Lilley KS, Salmond GP. 2009. The phage abortive infection system, ToxIN, functions as a protein-RNA toxin-antitoxin pair. *Proc Natl Acad Sci U S A* 106:894–899. <https://doi.org/10.1073/pnas.0808832106>.
 18. Guegler CK, Laub MT. 2021. Shutdown of host transcription triggers a toxin-antitoxin system to cleave phage RNA and abort infection. *Mol Cell* <https://doi.org/10.1016/j.molcel.2021.03.027>.
 19. Harms A, Maisonneuve E, Gerdes K. 2016. Mechanisms of bacterial persistence during stress and antibiotic exposure. *Science* 354:aaf4268. <https://doi.org/10.1126/science.aaf4268>.
 20. Harms A, Brodersen DE, Mitarai N, Gerdes K. 2018. Toxins, targets, and triggers: an overview of toxin-antitoxin biology. *Mol Cell* 70:768–784. <https://doi.org/10.1016/j.molcel.2018.01.003>.
 21. Fraikin N, Goormaghtigh F, Van Melderen L. 2020. Type II toxin-antitoxin systems: evolution and revolutions. *J Bacteriol* 202:e00763-19. <https://doi.org/10.1128/JB.00763-19>.
 22. Arnoldini M, Mostowy R, Bonhoeffer S, Ackermann M. 2012. Evolution of stress response in the face of unreliable environmental signals. *PLoS Comput Biol* 8:e1002627. <https://doi.org/10.1371/journal.pcbi.1002627>.
 23. Bobonis J, Mateus A, Pfalz B, Garcia-Santamarina S, Galardini M, Kobayashi C, Stein F, Savitski MM, Eifenbein JR, Andrews-Polymeris H, Typas A. 2020. Bacterial retrons encode tripartite toxin/antitoxin systems. *bioRxiv* <https://doi.org/10.1101/2020.06.22.160168>.
 24. Bobonis J, Mitosch K, Mateus A, Kritikos G, Eifenbein JR, Savitski MM, Andrews-Polymeris H, Typas A. 2020. Phage proteins block and trigger retron toxin/antitoxin systems. *bioRxiv* <https://doi.org/10.1101/2020.06.22.160242>.
 25. Gao L, Altae-Tran H, Bohning F, Makarova KS, Segel M, Schmid-Burgk JL, Koob J, Wolf YI, Koonin EV, Zhang F. 2020. Diverse enzymatic activities mediate antiviral immunity in prokaryotes. *Science* 369:1077–1084. <https://doi.org/10.1126/science.aba0372>.
 26. Millman A, Bernheim A, Stokar-Avihail A, Fedorenko T, Voickek M, Leavitt A, Oppenheimer-Shaanan Y, Sorek R. 2020. Bacterial retrons function in anti-phage defense. *Cell* 183:1551–1561.e12. <https://doi.org/10.1016/j.cell.2020.09.065>.
 27. LeRoux M, Culviner PH, Liu YJ, Littlehale ML, Laub MT. 2020. Stress can induce transcription of toxin-antitoxin systems without activating toxin. *Mol Cell* 79:280–292.e8. <https://doi.org/10.1016/j.molcel.2020.05.028>.
 28. Schumacher MA, Balani P, Min J, Chinnam NB, Hansen S, Vulčić M, Lewis K, Brennan RG. 2015. HipBA-promoter structures reveal the basis of heritable multidrug tolerance. *Nature* 524:59. <https://doi.org/10.1038/nature14662>.
 29. Verstraeten N, Knapen WJ, Kint CI, Liebens V, Van den Bergh B, Dewachter L, Michiels JE, Fu Q, David CC, Fierro AC, Marchal K, Beirlant J, Versee W, Hofkens J, Jansen M, Fauvart M, Michiels J. 2015. O₂ and membrane depolarization are part of a microbial bet-hedging strategy that leads to antibiotic tolerance. *Mol Cell* 59:9–21. <https://doi.org/10.1016/j.molcel.2015.05.011>.
 30. Meylan S, Andrews IW, Collins JJ. 2018. Targeting antibiotic tolerance, pathogen by pathogen. *Cell* 172:1228–1238. <https://doi.org/10.1016/j.cell.2018.01.037>.
 31. Balaban NQ, Helaine S, Lewis K, Ackermann M, Aldridge B, Andersson DI, Brynildsen MP, Bumann D, Camilli A, Collins JJ, Dehio C, Fortune S, Ghigo JM, Hardt WD, Harms A, Heinemann M, Hung DT, Jenal U, Levin BR, Michiels J, Storz G, Tan MW, Tenson T, Van Melderen L, Zinkernagel A. 2019. Definitions and guidelines for research on antibiotic persistence. *Nat Rev Microbiol* 17:441–448. <https://doi.org/10.1038/s41579-019-0196-3>.
 32. Balaban NQ, Merrin J, Chait R, Kowalik L, Leibler S. 2004. Bacterial persistence as a phenotypic switch. *Science* 305:1622–1625. <https://doi.org/10.1126/science.1099390>.
 33. Van den Bergh B, Fauvart M, Michiels J. 2017. Formation, physiology, ecology, evolution and clinical importance of bacterial persisters. *FEMS Microbiol Rev* 41:219–251. <https://doi.org/10.1093/femsre/fux001>.
 34. Defraigne V, Fauvart M, Michiels J. 2018. Fighting bacterial persistence: current and emerging anti-persister strategies and therapeutics. *Drug Resist Updat* 38:12–26. <https://doi.org/10.1016/j.drug.2018.03.002>.
 35. Dewachter L, Fauvart M, Michiels J. 2019. Bacterial heterogeneity and antibiotic survival: understanding and combatting persistence and heteroresistance. *Mol Cell* 76:255–267. <https://doi.org/10.1016/j.molcel.2019.09.028>.
 36. Bigger J. 1944. Treatment of staphylococcal infections with penicillin by intermittent sterilisation. *Lancet* 244:497–500. [https://doi.org/10.1016/S0140-6736\(00\)74210-3](https://doi.org/10.1016/S0140-6736(00)74210-3).
 37. Pontes MH, Groisman EA. 2019. Slow growth determines nonheritable antibiotic resistance in *Salmonella enterica*. *Sci Signal* 12:eaax3938. <https://doi.org/10.1126/scisignal.aax3938>.
 38. Levin-Reisman I, Ronin I, Gefen O, Braniss I, Shoshani N, Balaban NQ. 2017. Antibiotic tolerance facilitates the evolution of resistance. *Science* 355:826–830. <https://doi.org/10.1126/science.aaj2191>.
 39. Wakamoto Y, Dhar N, Chait R, Schneider K, Signorino-Gelo F, Leibler S, McKinney JD. 2013. Dynamic persistence of antibiotic-stressed *Mycobacterium*. *Science* 339:91–95. <https://doi.org/10.1126/science.1229858>.
 40. Pu Y, Zhao Z, Li Y, Zou J, Ma Q, Zhao Y, Ke Y, Zhu Y, Chen H, Baker MAB, Ge H, Sun Y, Xie XS, Bai F. 2016. Enhanced efflux activity facilitates drug tolerance in dormant bacterial cells. *Mol Cell* 62:284–294. <https://doi.org/10.1016/j.molcel.2016.03.035>.
 41. Moyed HS, Bertrand KP. 1983. *hipA*, a newly recognized gene of *Escherichia coli* K-12 that affects frequency of persistence after inhibition of murein synthesis. *J Bacteriol* 155:768–775. <https://doi.org/10.1128/JB.155.2.768-775.1983>.
 42. Korch SB, Henderson TA, Hill TM. 2003. Characterization of the *hipA7* allele of *Escherichia coli* and evidence that high persistence is governed by (p)ppGpp synthesis. *Mol Microbiol* 50:1199–1213. <https://doi.org/10.1046/j.1365-2958.2003.03779.x>.
 43. Korch SB, Hill TM. 2006. Ectopic overexpression of wild-type and mutant *hipA* genes in *Escherichia coli*: effects on macromolecular synthesis and persister formation. *J Bacteriol* 188:3826–3836. <https://doi.org/10.1128/JB.01740-05>.
 44. Evdokimov A, Voznesensky I, Fennell K, Anderson M, Smith JF, Fisher DA. 2009. New kinase regulation mechanism found in *HipBA*: a bacterial persistence switch. *Acta Crystallogr D Biol Crystallogr* 65:875–879. <https://doi.org/10.1107/S0907444909018800>.
 45. Schumacher MA, Piro KM, Xu W, Hansen S, Lewis K, Brennan RG. 2009. Molecular mechanisms of *HipA*-mediated multidrug tolerance and its neutralization by *HipB*. *Science* 323:396–401. <https://doi.org/10.1126/science.1163806>.
 46. Schumacher MA, Min J, Link TM, Guan Z, Xu W, Ahn Y-H, Soderblom EJ, Kurie JM, Evdokimov A, Moseley MA, Lewis K, Brennan RG. 2012. Role of unusual P-loop ejection and autophosphorylation in *HipA*-mediated persistence and multidrug tolerance. *Cell Rep* 2:518–525. <https://doi.org/10.1016/j.celrep.2012.08.013>.
 47. Wen Y, Behiels E, Felix J, Elegeert J, Vergauwen B, Devreese B, Savvides SN. 2014. The bacterial antitoxin *HipB* establishes a ternary complex with operator DNA and phosphorylated toxin *HipA* to regulate bacterial persistence. *Nucleic Acids Res* 42:10134–10147. <https://doi.org/10.1093/nar/gku665>.
 48. Wen Y, Sobott F, Devreese B. 2016. ATP and autophosphorylation driven conformational changes of *HipA* kinase revealed by ion mobility and crosslinking mass spectrometry. *Anal Bioanal Chem* 408:5925–5933. <https://doi.org/10.1007/s00216-016-9709-3>.
 49. Hanks SK, Quinn AM, Hunter T. 1988. The protein kinase family: conserved features and deduced phylogeny of the catalytic domains. *Science* 241:42–52. <https://doi.org/10.1126/science.3291115>.
 50. Stancik IA, Sestak MS, Ji B, Axelson-Fisk M, Franjevic D, Jers C, Domazet-Loso T, Mijakovic I. 2018. Serine/threonine protein kinases from Bacteria, Archaea and Eukarya share a common evolutionary origin deeply rooted in the tree of life. *J Mol Biol* 430:27–32. <https://doi.org/10.1016/j.jmb.2017.11.004>.

51. Germain E, Castro-Roa D, Zenkin N, Gerdes K. 2013. Molecular mechanism of bacterial persistence by HipA. *Mol Cell* 52:248–254. <https://doi.org/10.1016/j.molcel.2013.08.045>.
52. Kaspy I, Rotem E, Weiss N, Ronin I, Balaban NQ, Glaser G. 2013. HipA-mediated antibiotic persistence via phosphorylation of the glutamyl-tRNA-synthetase. *Nat Commun* 4:3001. <https://doi.org/10.1038/ncomms4001>.
53. Winther KS, Roghanian M, Gerdes K. 2018. Activation of the stringent response by loading of RelA-tRNA complexes at the ribosomal A-site. *Mol Cell* 70:95–105.e4. <https://doi.org/10.1016/j.molcel.2018.02.033>.
54. Bokinsky G, Baidoo EE, Akella S, Burd H, Weaver D, Alonso-Gutierrez J, García-Martín H, Lee TS, Keasling JD. 2013. HipA-triggered growth arrest and β -lactam tolerance in *Escherichia coli* are mediated by RelA-dependent ppGpp synthesis. *J Bacteriol* 195:3173–3182. <https://doi.org/10.1128/JB.02210-12>.
55. Correia FF, D'Onofrio A, Rejtar T, Li L, Karger BL, Makarova K, Koonin EV, Lewis K. 2006. Kinase activity of overexpressed HipA is required for growth arrest and multidrug tolerance in *Escherichia coli*. *J Bacteriology* 188:8360–8367. <https://doi.org/10.1128/JB.01237-06>.
56. Semanski M, Germain E, Bratl K, Kiessling A, Gerdes K, Macek B. 2018. The kinases HipA and HipA7 phosphorylate different substrate pools in *Escherichia coli* to promote multidrug tolerance. *Sci Signal* 11:eaat5750. <https://doi.org/10.1126/scisignal.aat5750>.
57. Huang CY, Gonzalez-Lopez C, Henry C, Mijakovic I, Ryan KR. 2020. hipBA toxin-antitoxin systems mediate persistence in *Caulobacter crescentus*. *Sci Rep* 10:2865. <https://doi.org/10.1038/s41598-020-59283-x>.
58. Zhou X, Eckart MR, Shapiro L. 2021. A bacterial toxin perturbs intracellular amino acid balance to induce persistence. *mBio* 12:e03020-20. <https://doi.org/10.1128/mBio.03020-20>.
59. Vang Nielsen S, Turnbull KJ, Roghanian M, Bærentsen R, Semanski M, Brodersen DE, Macek B, Gerdes K. 2019. Serine-threonine kinases encoded by split hipA homologs inhibit tryptophanyl-tRNA synthetase. *mBio* 10:e01138-19. <https://doi.org/10.1128/mBio.01138-19>.
60. Maeda Y, Lin C-Y, Ishida Y, Inouye M, Yamaguchi Y, Phadtare S. 2017. Characterization of Yjj toxin of *Escherichia coli*. *FEMS Microbiol Lett* 364:fnx086. <https://doi.org/10.1093/femsle/fnx086>.
61. Taylor SS, Keshwani MM, Steichen JM, Kornev AP. 2012. Evolution of the eukaryotic protein kinases as dynamic molecular switches. *Philos Trans R Soc Lond B Biol Sci* 367:2517–2528. <https://doi.org/10.1098/rstb.2012.0054>.
62. Rocker A, Meinhardt A. 2015. A cis-acting antitoxin domain within the chromosomal toxin-antitoxin module EzeT of *Escherichia coli* quenches toxin activity. *Mol Microbiol* 97:589–604. <https://doi.org/10.1111/mmi.13051>.
63. Kelley LA, Mezulis S, Yates CM, Wass MN, Sternberg MJ. 2015. The Phyre2 web portal for protein modeling, prediction and analysis. *Nat Protoc* 10:845–858. <https://doi.org/10.1038/nprot.2015.053>.
64. Ubeda C, Maiques E, Barry P, Matthews A, Tormo MA, Lasa I, Novick RP, Penades JR. 2008. SaPI mutations affecting replication and transfer and enabling autonomous replication in the absence of helper phage. *Mol Microbiol* 67:493–503. <https://doi.org/10.1111/j.1365-2958.2007.06027.x>.
65. Tormo-Mas MA, Mir I, Shrestha A, Tallent SM, Campoy S, Lasa I, Barbe J, Novick RP, Christie GE, Penades JR. 2010. Moonlighting bacteriophage proteins derepress staphylococcal pathogenicity islands. *Nature* 465:779–782. <https://doi.org/10.1038/nature09065>.
66. Fillol-Salom A, Martínez-Rubio R, Abdulrahman RF, Chen J, Davies R, Penades JR. 2018. Phage-inducible chromosomal islands are ubiquitous within the bacterial universe. *ISME J* 12:2114–2128. <https://doi.org/10.1038/s41396-018-0156-3>.
67. Ciges-Tomas JR, Alite C, Humphrey S, Donderis J, Bowring J, Salvatella X, Penades JR, Marina A. 2019. The structure of a polygamous repressor reveals how phage-inducible chromosomal islands spread in nature. *Nat Commun* 10:3676. <https://doi.org/10.1038/s41467-019-11504-2>.
68. Fillol-Salom A, Bacarizo J, Alqasmi M, Ciges-Tomas JR, Martínez-Rubio R, Roszak AW, Cogdell RJ, Chen J, Marina A, Penades JR. 2019. Hijacking the hijackers: *Escherichia coli* pathogenicity islands redirect helper phage packaging for their own benefit. *Mol Cell* 75:1020–1030.e4. <https://doi.org/10.1016/j.molcel.2019.06.017>.
69. Mitarai N. 2020. How pirate phage interferes with helper phage: comparison of the two distinct strategies. *J Theor Biol* 486:110096. <https://doi.org/10.1016/j.jtbi.2019.110096>.
70. Iyer LM, Babu MM, Aravind L. 2006. The HIRAN domain and recruitment of chromatin remodeling and repair activities to damaged DNA. *Cell Cycle* 5:775–782. <https://doi.org/10.4161/cc.5.7.2629>.
71. Kile AC, Chavez DA, Bacal J, Eldirany S, Korzhnev DM, Bezsonova I, Eichman BF, Cimprich KA. 2015. HLTf's ancient HIRAN domain binds 3' DNA ends to drive replication fork reversal. *Mol Cell* 58:1090–1100. <https://doi.org/10.1016/j.molcel.2015.05.013>.
72. Hishiki A, Sato M, Hashimoto H. 2020. Structure of HIRAN domain of human HLTf bound to duplex DNA provides structural basis for DNA unwinding to initiate replication fork regression. *J Biochem* 167:597–602. <https://doi.org/10.1093/jb/mvaa008>.
73. Quinet A, Lemacon D, Vindigni A. 2017. Replication fork reversal: players and guardians. *Mol Cell* 68:830–833. <https://doi.org/10.1016/j.molcel.2017.11.022>.
74. Dy RL, Richter C, Salmond GP, Fineran PC. 2014. Remarkable mechanisms in microbes to resist phage infections. *Annu Rev Virol* 1:307–331. <https://doi.org/10.1146/annurev-virology-031413-085500>.
75. Lopatina A, Tal N, Sorek R. 2020. Abortive infection: bacterial suicide as an antiviral immune strategy. *Annu Rev Virol* 7:371–384. <https://doi.org/10.1146/annurev-virology-011620-040628>.
76. Mondragon A. 1995. Unraveling transposition: gamma delta resolvase in complex with DNA. *Structure* 3:755–758.
77. Artymiuk PJ, Ceska TA, Suck D, Sayers JR. 1997. Prokaryotic 5'-3' exonucleases share a common core structure with gamma-delta resolvase. *Nucleic Acids Res* 25:4224–4229. <https://doi.org/10.1093/nar/25.21.4224>.
78. Black DS, Irwin B, Moyed HS. 1994. Autoregulation of hip, an operon that affects lethality due to inhibition of peptidoglycan or DNA synthesis. *J Bacteriology* 176:4081–4091. <https://doi.org/10.1128/jb.176.13.4081-4091.1994>.
79. Potter SC, Luciani A, Eddy SR, Park Y, Lopez R, Finn RD. 2018. HMMER web server: 2018 update. *Nucleic Acids Res* 46:W200–W204. <https://doi.org/10.1093/nar/gky448>.
80. Sievers F, Higgins DG. 2018. Clustal Omega for making accurate alignments of many protein sequences. *Protein Sci* 27:135–145. <https://doi.org/10.1002/pro.3290>.
81. Waterhouse AM, Procter JB, Martin DM, Clamp M, Barton GJ. 2009. Jalview version 2—a multiple sequence alignment editor and analysis workbench. *Bioinformatics* 25:1189–1191. <https://doi.org/10.1093/bioinformatics/btp033>.
82. Letunic I, Bork P. 2019. Interactive Tree Of Life (iTOL) v4: recent updates and new developments. *Nucleic Acids Res* 47:W256–W259. <https://doi.org/10.1093/nar/gkz239>.
83. Minh BQ, Nguyen MA, von Haeseler A. 2013. Ultrafast approximation for phylogenetic bootstrap. *Mol Biol Evol* 30:1188–1195. <https://doi.org/10.1093/molbev/mst024>.
84. Trifinopoulos J, Nguyen LT, von Haeseler A, Minh BQ. 2016. W-IQ-TREE: a fast online phylogenetic tool for maximum likelihood analysis. *Nucleic Acids Res* 44:W232–W235. <https://doi.org/10.1093/nar/gkw256>.
85. Minh BQ, Schmidt HA, Chernomor T, Schrempf M, Woodhams MD, von Haeseler A, Lanfear R. 2020. IQ-TREE 2: new models and efficient methods for phylogenetic inference in the genomic era. *Mol Biol Evol* 37:1530–1534. <https://doi.org/10.1093/molbev/msaa015>.
86. Rice P, Longden I, Bleasby A. 2000. EMBOSS: the European Molecular Biology Open Software Suite. *Trends Genet* 16:276–277. [https://doi.org/10.1016/s0168-9525\(00\)02024-2](https://doi.org/10.1016/s0168-9525(00)02024-2).
87. Dodd IB, Egan JB. 1990. Improved detection of helix-turn-helix DNA-binding motifs in protein sequences. *Nucleic Acids Res* 18:5019–5026. <https://doi.org/10.1093/nar/18.17.5019>.
88. Hansen S, Vulic M, Min J, Yen TJ, Schumacher MA, Brennan RG, Lewis K. 2012. Regulation of the *Escherichia coli* HipBA toxin-antitoxin system by proteolysis. *PLoS One* 7:e39185. <https://doi.org/10.1371/journal.pone.0039185>.
89. Sievers F, Willm A, Dineen D, Gibson TJ, Karplus K, Li W, Lopez R, McWilliam H, Remmert M, Soding J, Thompson JD, Higgins DG. 2011. Fast, scalable generation of high-quality protein multiple sequence alignments using Clustal Omega. *Mol Syst Biol* 7:539. <https://doi.org/10.1038/msb.2011.75>.